Application of Physiological and Pathological Wall Shear Stress to Endocardial Endothelial Cells Triggers Complex Signaling Pathways

Kathleen N. Brown[1], Hong Kim T. Phan[1], Tasneem Mustafa[1], Jennifer P. Connell[1], Philippe Sucosky[2], Sundeep G. Keswani[3,4], and K. Jane Grande-Allen[1]

Affiliations

[1]Department of Bioengineering, Rice University, Houston, TX

[2]Department of Mechanical Engineering, Kennesaw State University, Kennesaw, GA

[3]Department of Surgery, Baylor College of Medicine, Houston, TX

[4]Division of Pediatric Surgery, Department of Surgery, Texas Children's Hospital, Houston, TX

Abbreviated title: Shear stress driven EEC signaling

Address for correspondence:

K. Jane Grande-Allen, Ph.D.

Department of Bioengineering

Rice University

6100 Main St., MS 142

Houston, TX 77005

Phone: 713-348-3704

Email: grande@rice.edu

Abstract

Discrete subaortic stenosis (DSS) is a congenital heart disease characterized by the formation of a fibrotic membrane below the aortic valve. The underlying cellular mechanisms of this disease are currently unknown. As one of the distinguishing features of DSS is the elevated pressure gradient in the left ventricular outflow tract, it is theorized that the membrane formation is caused by elevated wall shear stress applied to the endocardial endothelial cells (EECs), triggering fibrosis. To relate shear stress to an EEC fibrotic phenotype, we applied fluid shear stress to EECs at physiological and pathological shear rates using a cone-and-plate device. Upon characterization of the EECs after the shear experiments, elevated shear stress triggered cell alignment as well as endothelial-to-mesenchymal transformation (EndMT) signaling pathways driven by upregulation of *SNAI1* gene expression. The EECs were then treated with a small molecule inhibitor of Snail1 protein, CYD19, to attempt to attenuate EndMT signaling, and subsequently subjected to pathological shear stress. We found the Snail1 inhibitor did downregulate selected markers of EndMT signaling, although only transiently. Interestingly, the application of shear stress had a far greater effect on the EEC gene and protein expression in comparison to the Snail1 inhibition. Our findings are the first insight to EEC specific response to high shear stress. Further study should reveal the mechanisms that drive fibrosis and the formation of the DSS membrane.

Introduction

Discrete subaortic stenosis (DSS) is a rare, congenital heart disease that is characterized by formation of a fibrotic membrane in the subvalvular region of the left ventricular outflow tract (LVOT) of the heart. This membrane then obstructs blood flow through the aortic valve. Up to 10% of patients with congenital heart disease present with a LVOT obstruction (1), and DSS accounts for up to 15% of these cases (2). Patients that present with DSS experience a range of symptoms including loss of consciousness, shortness of breath, and chest pain (2). The DSS membrane, when left untreated, is progressive in nature and will increasingly grow to restrict blood flow through the LVOT, resulting in high rates of morbidity and mortality (3). To date, the only option for treatment of DSS is surgical removal of the membrane. As this requires open heart surgery, physicians typically wait for the membrane to progress into an “optimal surgical window” (1). Distressingly, up to 29% of DSS patients have the membrane reoccur within 13 years of their first membrane resection (3).

DSS is a debilitating disease that affects very young patients, and the underlying cellular mechanism that drives membrane formation is unknown. There are clues in the disease presentation, however, that could help scientists uncover the signaling pathways that cause DSS. For example, the membrane that forms is composed of fibrotic extracellular matrix proteins and the left ventricular wall of patients with DSS is thickened; these changes are hallmarks of cardiac fibrosis. Additionally, the aortoseptal angle is steeper than normal in patients with DSS, which could contribute to elevated wall shear stress within the LVOT (4–6). Although the disease does not appear to be genetically inherited, patients with DSS often present with multiple congenital heart diseases, and thus this condition may be linked to a genetic mutation that has not been discovered. Despite physicians and scientists speculating about the cause of DSS (7,8), there are no experimental studies that have investigated the cellular and molecular mechanisms of the disease. Here, we have created an *in vitro* model of

DSS that mimics the elevated wall shear stress levels that are estimated from echocardiographic measurements in DSS patients. In the LVOT, physiological wall shear stress range from 10-15 dynes/cm^2, and DSS patients experience wall shear stresses that range from 30-55 dynes/cm^2 (1,4,7,9). To our knowledge, this is the first *in vitro* model used to investigate DSS pathology as it relates to wall shear stress.

In this study, we aimed to investigate the role of supra-physiological wall shear stresses on endocardial endothelial cells (EECs), the cells that line the LVOT. We isolated EECs from porcine hearts, exposed the cells to varying levels of shear stresses using a previously reported cone-and-plate device (10), and then characterized the cellular inflammatory and fibrotic responses.

Materials and Methods

Endocardial endothelial cell isolation & culture

Endocardial endothelial cells were isolated from porcine hearts, as described in Chapter 3. After isolating the cells, and sorting the cells twice for CD31, the cells were frozen and stored in liquid nitrogen until testing. Prior to shear stress experiments, cells were thawed and seeded into 75 cm^2 tissue culture treated flasks. The cell cultures were supplemented with Endothelial Growth Medium-2 (EGM-2, Lonza #CC-3162), which was changed every other day until the cells reached ~75% confluence. The cells were then passaged and plated in 60 mm tissue culture treated petri dishes (Thermo Fisher, #150462) at a density of 0.8 x10^6 cells per dish. The cells were grown to confluency prior to further experimentation.

Applying shear stress with a cone-and-plate device

A cone-and-plate device was used to apply shear stress in our experiments (**Figure 1**) as previously described (10). The cone assembly was custom machined at the Houston

Methodist Hospital machine shop (Houston, TX). The cone and shaft were machined from titanium; the cover for the cone was machined from Teflon. The cone had a smooth surface with an angle of 0.5°. The gap height of the cone could be adjusted using the collar shaft. The shear stress applied by the cone was determined as $\tau = \mu \cdot \frac{\omega \cdot r}{h_0 + r \cdot \alpha}$, where τ = wall shear stress, μ = dynamic viscosity of fluid, ω = angular velocity of the cone, r = radius of the cone, h_0= gap height, and α = angle between the cone-and-plate, as previously reported (11).

To sterilize the cones prior to experimentation, the cones were exposed to UV light for a minimum of 3 hours. The gap height of the cone was set by loading the cone onto a petri dish containing two #1 coverslips, stacked atop each other to achieve a gap height of 300 μm, and then tightening the collar shaft of the cone. The adjusted cone was then loaded onto a petri dish containing EECs and 2.0 mL of cell culture medium. The cone-and-plate components were then transferred to a magnetic stir plate with a controllable rotational speed (Cole-Parmer, #EW-84003-82). Using the equation above, the desired shear stress was used to determine the required rotational setting of the stir plate as shown in **Table 1**.

Cell imaging and analysis

Brightfield images of the cells were obtained before and after the application of shear stress. Samples were imaged on a Nikon Ti2 eclipse microscope. After image acquisition, image processing was performed in ImageJ. Alignment analysis was performed in ImageJ using the OrientationJ plugin.

Quantitative polymerase chain reaction

After shear stress experiments, total RNA was isolated from samples by incubating each sample with 300 μL TRIzol reagent (Thermo Fisher, #15596018) for 10 minutes, and then

using a cell scraper to scrape the cells into the solution. The total RNA was then purified from the TRIzol lysate using the Direct-zol RNA MicroPrep Kit from Zymo Research (#R2062), following the manufacturer's instructions. After purification, RNA quality and quantity was evaluated and recorded using the NanoDrop 2000. RNA samples were stored at -80°C until further processing. cDNA was synthesized from the RNA samples at a starting amount of 200 ng RNA using the High Capacity cDNA Reverse Transcription Kit (Thermo Fisher, #4368813) per manufacturer's instructions. cDNA samples were stored at -20˚C. Quantitative reverse transcriptase polymerase chain reaction (qPCR) was performed using the iTaq Universal Probes Supermix (Bio-Rad, #1725134) with Taqman porcine primers specific to CD31 (probe ID: Ss03392600_u1), ACTA2 (Ss04245588_m1), VCAM1 (Ss03390912_m1), ICAM1 (Ss03392385_m1), Vimentin (Ss04330801_gH), YAP1 (Ss06912139_m1), von Willebrand Factor (Ss04322692_m1), COL1A2 (Ss03375009_u1), COL3A1 (Ss04323794_m1), and GAPDH (Ss03374854_g1). qPCR for SNAI1 expression was performed using the RT^2 SYBR Green qPCR Mastermix (Qiagen, #330503) with RT^2 qPCR Primer Assay porcine primers specific to SNAI1 (GeneGlobe ID: PPS07880A), and GAPDH (PPS00192A).

Fibrosis profiler array

We utilized the RT^2 Profiler PCR Array Pig Fibrosis from Qiagen (#330231, Gene GlobeID: PASS-120ZD). The array was supplied as a pre-loaded qPCR plate. RNA samples were isolated and purified as previously described, cDNA was synthesized using the RT^2 First Strand Kit (Qiagen, # 330404). All kits were used according to manufacturer's instructions. The analysis of this array was performed on the Qiagen website, on the GeneGlobe data analysis tab.

Small molecule inhibition of Snail

A small molecule inhibitor of Snail, CYD19, was applied to cells. The chemical name for the molecule is N-(2-Amino-4-fluorophenyl)-4-(((4-((5-methyl-1H-pyrazol-3-yl)amino)pyrrolo[2,1-f][1,2,4]triazin-2-yl)thio)methyl)benzamide and the molecule was purchased from Aobious (#AOB11460). The molecule was dissolved in DMSO and stored at a stock solution concentration of 4.0937 μM and stored at room temperature. CYD19 was added to the cells at a concentration of 50 nM, the dosage recommended by a previously published study (12). To account for the effects that DMSO might have on the cells, we included vehicle controls.

Flow cytometry

To evaluate the protein expression of the EECs, flow cytometry was performed. To lift the cells, the dish of cells was rinsed with PBS and then 5 mL of Accutase (Sigma-Aldrich, #A6964) was added to each 60 mm dish and incubated for 10 minutes at 37°C. After incubating, the dishes were gently tapped to lift the cells. The Accutase solution was transferred to a conical tube and then centrifuged for 5 minutes at 150 x*g* to obtain a cell pellet. The cells were then resuspended in 1% fetal bovine serum (FBS, Fisher Scientific, #FB12999102) in phosphate buffered saline (PBS) at a density of 1 x10^6 cells per 100 μL. At this point, the cells were divided into different microcentrifuge tubes for the testing conditions. Each sample was first incubated with extracellular antibodies, then the samples were fixed, and then incubated with intracellular antibodies. The workflow for this process is described below.

For extracellular antibodies, the antibodies and corresponding isotype controls were added to their respective samples' tubes at concentrations recommended by the manufacturer (see **Table 2**). The samples were protected from light and incubated with the antibody at room temperature for 15 minutes. After incubation, 1 mL of 1% FBS in PBS was added to each tube

for washing. The samples were centrifuged to obtain a cell pellet, then the supernatant was removed using a micropipette tip. The samples were washed again by resuspending the cell pellet into 1 mL 1% FBS in PBS to each tube and centrifuged again to obtain a cell pellet.

For intracellular antibodies, the cells were resuspended in 1 mL of 4% paraformaldehyde and incubated at 4˚C for 20 minutes to fix the cells. The cells were centrifuged to obtain a cell pellet. After fixation, the cells were permeabilized in a solution of 1% Tween20, 1% FBS in PBS at room temperature for 15 minutes. The cells were centrifuged to obtain a cell pellet. The cells were resuspended in 100 µL of the 1% Tween20, 1% FBS in PBS solution. The antibodies and corresponding isotype controls were then added to their respective samples tubes at concentrations recommended by the manufacturer (see **Table 2**). The samples were protected from light and incubated with the antibody at room temperature for 45 minutes. The cells were centrifuged to obtain a cell pellet. The samples were washed again by resuspending the cell pellet into 1 mL 1% FBS in PBS to each tube and centrifuged again to obtain a cell pellet.

The stained cells were resuspended in ~500 µL 1% FBS in PBS and transferred to polystyrene 5 mL flow cytometry tubes (MTC Bio, #T9010). The samples were placed on ice and protected from light until flow cytometry could be performed. Flow cytometry was performed on a Sony MA900 flow cytometer, and analysis was performed in FlowJo Version 7.

Statistical analysis

Statistical analysis was performed in GraphPad Prism Version 9.4.1. To analyze the initial PCR results, fold changes were calculated using the ΔΔCT method. Briefly, the CT values of experimental conditions were normalized to expression of GAPDH, then normalized to the expression of the control sample. A one-way ANOVA test was performed on the data, with post-hoc analysis performed using Tukey's test. All data was graphed as means ±

standard deviation. For the small molecule inhibitor study, a two-way ANOVA was performed on the data, with post-hoc analysis performed using Tukey's test. Results with p-value < 0.05 were considered statistically significant.

Results

Shear stress drives EEC alignment

To apply continuous, uniform laminar shear stress to EECs, we utilized the cone-and-plate device shown in **Figure 1.** After exposing the cells to either static conditions (no shear stress), low shear stress (15 dynes/cm^2), medium shear stress (20 dynes/cm^2), or high shear stress (35 dynes/cm^2), brightfield images of the EECs were captured at different locations around the petri dish, as shown in **Figure 2**. We observed that after application of shear stress, the cells aligned to the direction of the fluid rotation. In **Figure 3**, brightfield images of the EECs demonstrate the cells alignment before and after the application of shear stress. The degree of orientation of the cells was analyzed with the OrientationJ plugin in ImageJ. This plugin produced orientation data as well as images of EECs that were overlain with a color map corresponding to the degree of orientation. The analyzed images and the color map are shown in the last column of **Figure 3**. We observed that the cells exhibited different degrees of alignment depending on the shear rate applied. To compare this effect, we analyzed the distribution of orientation of 10 samples for each shear condition and graphed the pixel distributions of each sample in **Figure 4**. For these graphs, each line represents a different sample within each shear condition, with all images captured from the same region of the petri dish. In the static condition, the cells have a non-uniform distribution of alignment. After applying low or medium magnitudes of shear stress, the cells are aligning in a uniform direction. Interestingly, in the high shear stress condition, the cells displayed a non-uniform alignment, similar to the static condition.

Shear stress drives time dependent gene expression

After exposing the EECs to shear stress, we isolated the RNA from the cells, and proceeded with qPCR to analyze the gene expression of the EECs in response to varying shear rates, as shown in **Figure 5**. We examined *CD31* as a representative endothelial marker, *ACTA2* as a marker of fibrosis, and *ICAM1* and *VCAM1* as inflammatory markers. The results shown in **Figure 5** demonstrate that the cellular response is dependent upon both shear rate and time. The endothelial marker, *CD31*, remains largely unchanged across time points and shear conditions, indicating that the endothelial cells maintained their phenotype throughout the experiment. The fibrotic marker *ACTA2*, which encodes for the protein α-smooth muscle actin, was significantly downregulated in response to shear, but only at the 8-hour time point. The inflammatory marker, *ICAM1* was significantly upregulated at the 1.5-hour time point in response to shear, but did not demonstrate differences at later time points. However, *VCAM1* was significantly downregulated in response to shear at later time points (8 and 16 hours). The *VCAM1* results also varied based on the shear rate, indicating that higher shear stress affected the EECs differently than did lower shear stress.

Fibrosis array suggests role for Snail in shear stimulated EECs

Based on these initial findings of cellular response to the shear stress, we sought to cast a wider net to gain further insights. To do so, we used a fibrosis PCR profiler array that analyzed the expression of 84 fibrotic genes. Using the profiler array, we compared the gene expression of statically-cultured EECs to those exposed to high shear stress for 1.5, 8, and 16 hours. The volcano plots of genes that were significantly upregulated and downregulated are shown in **Figure 6**. In these plots, the vertical lines are the thresholds set for the minimum fold change of interest, and the horizontal line is the minimum significance threshold of interest.

Genes that were located in the upper left and right quadrants of the graphs were identified as the genes of interest. Comparing the volcano plots of the three time points, more genes were upregulated than downregulated in response to shear stress. A clustergram of the genes analyzed in the profiler array and the resulting gene expression of the samples compared is shown in **Figure 7**. At the top of the graph, the sample groups are labeled for static EECs, and EECs exposed to high shear stress for 1.5 hours, 8 hours, and 16 hours. We observed that there is uniformity of gene expression within each sample group.

Following the fibrosis profiler array analysis, we compared the genes that were significantly upregulated and downregulated in response to shear stress to assess signaling pathway trends. *SNAI1*, which encodes for a transcription factor, Snail1, was significantly upregulated (fold change was 26.6, p value < 0.01) at the earlier time point of 1.5 hours, whereas ECM genes such as *COL3A1* (fold change was 183.81, p value < 0.01), *COL1A2* (fold change was 38.86, p value < 0.05), and *DCN* (fold change was 90.73, p value < 0.05) were significantly upregulated at the later time point of 16 hours. Based on this data, we hypothesized that *SNAI1* was a mechanosensitive marker that was upregulated at early time points in response to shear, and thus initiated signaling pathways that lead to increased ECM production. We looked to the literature to investigate how these signaling markers could be linked, and we found that upregulation of gene expression for these markers are indicative of endothelial-to-mesenchymal transition (EndMT). During EndMT, endothelial cells that are exposed to specific developmental programming stimuli or pathological conditions undergo a transition to a mesenchymal phenotype, such as fibroblasts or smooth muscle cells (13–19). EndMT is a transition process, therefore cells undergoing EndMT can exhibit markers of both endothelial and mesenchymal cells at once (13,14,19,20). To detect early EndMT, one would look for an upregulation of mesenchymal genes and the proteins they encode for, such as α-smooth muscle actin protein (encoded by *ACTA2*), CD44 protein (encoded by *CD44*), and

Snail1 protein (encoded by *SNAI1*), and a downregulation of endothelial genes and the proteins they encode for, such as von Willebrand Factor protein (encoded by *VWF*), CD31 protein (encoded by *CD31*), and VE cadherin protein (encoded by *CDH5*) (13–15,18,19). At late stages of EndMT, one would look for an upregulation of different mesenchymal genes and the proteins they encode for, such as vimentin protein (encoded by *VIM*) and Notch3 protein (encoded by *NOTCH3*), an upregulation of ECM genes and the proteins they encode for, such as fibronectin (encoded by *FN1*), collagen III (encoded by *COL3A1*), and MMPs 2 and 9 (encoded by *MMP2* and *MMP9*, respectively), and a downregulation of endothelial genes and the proteins they encode for, such as CD31 and von Willebrand Factor (13–15,18,19). The typical signs of early and late EndMT were present in the EECs that we exposed to high shear stress, which led us to hypothesize that pathological shear stress induces EndMT signaling in EECs, initially driven by *SNAI1*.

Small molecule inhibition of Snail transiently influenced EndMT markers

To investigate this hypothesis, we researched small molecule inhibitors for the gene *SNAI1* or the protein it encodes for, Snail1, to try to disrupt the EndMT process we observed in EECs. We found a study that discovered the small molecule inhibitor CYD19, and demonstrated the ability of the molecule to inhibit Snail1 *in vitro* and *in vivo* with a post-translational modification that promotes degradation of the Snail1 protein through the ubiquitin-proteasome pathway (12). We then investigated the effects of inhibiting Snail1 by treating the EECs with 50 nM CYD19 or the vehicle control (DMSO) for 2 days, then proceeded with shear stress studies to apply static conditions, or high shear stress for 1.5 and 24 hours. We observed an initial shift in cell morphology between the CYD19-treated and the vehicle-treated cells, as shown in **Figure 8**. The vehicle-treated EECs have a very similar elongated and

swirling morphology to the EECs shown in previous figures, whereas the CYD19-treated EECs shifted morphology to become more round and cobblestone-like.

After application of shear stress, gene and protein expression of the samples were analyzed with RT-qPCR and flow cytometry, respectively. To analyze how the small molecule inhibitor would affect the cellular response of EECs, we evaluated the gene and protein expression for markers of EndMT (*SNAI1, ACTA2, VIM*), an inflammatory marker (*VCAM1*), and an endothelial marker (*CD31*). We used a two-way ANOVA to compare gene expression between treatment condition and shear condition within each time point.

As shown in **Figure 9**, at 1.5 hours, the gene expression of *SNAI1* was not significantly influenced by the CYD19 treatment or the application of high shear stress. However, this result was expected, as CYD19 inhibits Snail1 on the protein level. Correspondingly, at 1.5 hours Snail1 protein expression was significantly downregulated in response to CYD19 treatment, and was significantly downregulated in response to high shear stress. At 24 hours, *SNAI1* gene expression remained unchanged in response to both CYD19 treatment and to the application of shear stress. Interestingly, we observed an abundance of Snail1 protein expression across all of the samples at the 24 hour time point (70-80%) compared to the expression level at 1.5 hours (10-40%). This result indicates that the effects of CYD19 treatment had on the EECs at 1.5 hours by inhibiting Snail1 expression, and thereby inhibiting EndMT expression, appear to have waned by the 24 hour time point.

As shown in **Figure 10**, at 1.5 hours, *ACTA2* gene expression was not significantly influenced by the CYD19 treatment or the application of high shear stress. At 1.5 hours, α-smooth muscle actin (α-SMA) protein was significantly downregulated by the application of high shear stress and was not influenced by the CYD19 treatment. At 24 hours, the dominating effect on both gene and protein expression was the application of shear stress. For both *ACTA2* gene expression and α-SMA protein expression high shear stress downregulated

expression of these markers, while CYD19 treatment did not influence the expression levels of these markers. The amount of α-SMA protein expressed increased between 1.5 hours (1-3%) to 24 hours (20-60%) which again suggests that the effects of CYD19 have waned by this later time point.

As shown in **Figure 11**, at 1.5 hours *VIM* gene expression was not significantly influenced by the CYD19 treatment or the application of high shear stress. Vimentin protein expression at 1.5 hours was not influenced by the CYD19 treatment, however, vimentin was downregulated in response to high shear stress. At 24 hours, *VIM* gene expression was observed to have exceptionally significant downregulation in response to the application of high shear stress, while remaining uninfluenced by the CYD19 treatment. At 24 hours, vimentin protein expression was not significantly influenced by the CYD19 treatment or the application of high shear stress. Similar to previous markers, there is an abundance of vimentin protein expression across all conditions at the 24 hour time point (< 90%) in comparison to the protein expression levels at 1.5 hours (40-80%). This result suggests that the effects of CYD19 in mitigating EndMT signaling have waned by the 24 hour time point.

As shown in **Figure 12**, at 1.5 hours *VCAM1* gene expression was interestingly significantly upregulated in response to CYD19 treatment, and was downregulated in response to high shear stress. VCAM1 protein expression at 1.5 hours was not significantly influenced by the CYD19 treatment or the application of high shear stress. At 24 hours, *VCAM1* gene expression was not significantly influenced by the CYD19 treatment, and was significantly downregulated in response to high shear stress. VCAM1 protein expression at 24 hours was not significantly influenced by the CYD19 treatment or the application of high shear stress. The dominating effect for both time points was downregulation of gene expression due to the application of high shear stress.

As shown in **Figure 13**, at 1.5 hours *CD31* gene expression was not influenced by the CYD19 treatment, and was significantly downregulated in response to shear stress. CD31 protein expression at 1.5 hours was not significantly influenced by the CYD19 treatment or the application of high shear stress. At 24 hours, *CD31* gene expression was significantly downregulated by CYD19 treatment and by exposure to high shear stress. CD31 protein expression at 24 hours was significantly upregulated by both the CYD19 treatment and the application of high shear stress. The amount of CD31 protein expressed between the time points was reduced at the 24 hour time point (30-65%) in comparison to the 1.5 hour time point (70-90%).

Discussion

In an effort to mimic the disease pathologies observed in DSS, we applied physiological and pathological levels of wall shear stress to EECs and characterized the cellular response through cellular alignment, gene expression, and protein expression. When observing the cellular alignment after application of shear stress, the EECs aligned to the direction of shear stress applied in low and medium shear rates, a phenomenon observed in many studies where shear stress is applied to endothelial cells. However, after applying high shear stress to EECs, we speculate that the EECs are transitioning to a mesenchymal phenotype as the cells were not as impacted by the application of shear stress. When comparing the low shear, medium shear, and high shear graphs, the cellular alignment is similar, with the most uniformity in cell alignment found in the medium shear condition.

After exposing EECs to high shear stress, the cells upregulated *SNAI1* gene expression, and gene expression of several ECM genes, which indicated the cells were undergoing endothelial-to-mesenchymal transition (EndMT). In the initial PCR analysis, the results demonstrated that the length of time the cells were exposed to shear and the shear

stress magnitude influenced the cellular response of the EECs. This led us to cast a wider net when analyzing the response of EECs to the application of shear stress by analyzing the cells with a fibrosis profiler. When selecting the samples to analyze with the profiler, we utilized the results of the initial PCR analysis to inform our decision. The results demonstrated EECs exposed to high shear stress at earlier time points would be the most relevant samples to include. Upon analyzing the EECs exposed to high shear stress for 1.5 hours, 8 hours, and 16 hours, the main findings were that *SNAI1* gene expression was significantly upregulated at 1.5 hours, and several ECM genes were upregulated at 16 hours, indicative of endothelial-to-mesenchymal transition (EndMT). EndMT is a process in which endothelial cells transition to mesenchymal cells (13,14,16,17). During this process, the endothelial cells lose their endothelial characteristics, and begin to express mesenchymal markers (13,14,16,17,21). The transition is a continuum, and endothelial cells undergoing EndMT co-express both endothelial and mesenchymal markers (13,18,19). While there are hallmarks of early and late EndMT, studies have shown this can vary depending on the pathological environment and cell type (14–16,18,19). Additionally, cells can undergo partial or full EndMT transition, further complicating detection of EndMT transition (13,18,19). An important regulator of EndMT is Snail1, a transcription factor known to induce EndMT (13,22,17,19,20,23–26). By treating the EECs with CYD19, a small molecule inhibitor of Snail1, we sought to uncover how Snail1 influences EECs exposed to pathological shear rates, and if inhibition of Snail1 could inhibit development of EndMT.

The results of inhibiting Snail1 expression via a small molecule inhibitor emphasize the complexity of the cellular signaling pathways that drive DSS formation. For example, the gene expression of *CD31* was downregulated in response to shear stress while the protein expression of CD31 was upregulated in response to shear stress. We also observed that the CYD19 inhibitor did downregulate Snail1 protein expression in comparison to the vehicle

control, but the effects of the small molecule inhibitor appear to wane by 24 hours. The results of the small molecule inhibitor study demonstrated the ability of CYD19 to inhibit Snail1, markers of EndMT, and markers of inflammation at earlier time points. However, the effects of CYD19 appear to be time dependent, and later time points showed upregulation of EndMT markers. While we did use the recommended dose of CYD19, it would be worthwhile to investigate dose dependent effects of CYD19 inhibition of EndMT signaling (12). It is also possible that to capture the full EndMT signaling process, additional cell types (cardiac fibroblasts, immune cells, etc) would need to be included in the disease model to recapitulate promotion of EndMT. Additionally, while we investigated cellular response to shear stress between 1.5 hours and 24 hours, it would be worthwhile to extend these experiments to longer time points to understand how time dependency affects EndMT promotion as well.

The application of high shear stress largely determined cellular response of EECs. The small molecule inhibitor study yielded interesting results, however, we were surprised that the dominating effect of shear stress drove gene expression changes, rather than Snail1 inhibition. In the results, the application of high shear stress governed the regulation of gene and protein expression of the EECs. This insight is helpful for future studies, as the application of shear stress is vital to include when modeling diseases of the heart.

This is the first study to apply supra-physiological levels of wall shear stress to EECs and characterize their response as it related to DSS formation. EECs have been implicated in several cardiac diseases, yet the available shear stress studies have focused primarily on modeling behavior of HUVECs in response to pathological shear rates (20,27). EECs have a unique phenotype, as proteomics analyses have demonstrated that EECs express a different phenotype from aortic endothelial cells, and even vary their phenotype throughout the regions of the heart (28–30). It is well understood that abnormal shear stress induces EndMT in HUVECs and in aortic valve endothelial cells, and may contribute to vascular disease

formation (15,18,23,31–36). However, studies need to be conducted to understand how EECs respond to pathological shear stress. Recently, EECs were included in a study investigating the role of shear stress in the formation of endocardial fibroelastosis (EFE) (20). This study was the first work to apply abnormal shear stress to EECs, and the investigators found that EECs exposed to abnormal shear conditions showed signs of undergoing EndMT through the co-expression of endothelial and mesenchymal markers and the increased expression of Snail1, which they concluded contributes to EFE (20). This important work emphasizes the importance of including EECs in cardiovascular disease models, as the specific phenotype and resulting signaling pathways of EECs are unique.

We observed that high shear stress does drive up *SNAI1* expression and drive down *CD31* expression in EECs, indicating EndMT. However, we did not see this reflected in mesenchymal markers, which could indicate the studies were not conducted for a long enough time point to capture the full EndMT process. There may be a more sophisticated signaling pathway at play, and this signaling mechanism should be investigated further. In the present study, we provided novel insights into the EEC specific response to physiological and pathological levels of shear stress. Further investigation is required to uncover the complex signaling mechanisms of the fibrotic membrane formation observed in DSS.

Conclusions

The cellular signaling pathways that govern gene and protein expression are complex to evaluate and understand. We demonstrated the effects that shear stress has on EECs, and attempted to fully characterize the cellular expression profiles of sheared EECs with a PCR profiler array. This led us to inhibit Snail1 with a small molecule inhibitor and apply shear stress to the cells once more. The gene expression and protein expression of endothelial, EndMT, inflammatory, and ECM markers were evaluated. We discovered that CYD19 does inhibit

EndMT and inflammatory proteins at early time points, while improving expression of endothelial markers. The gene and protein expression profiles did vary, which emphasizes the challenge of evaluating cellular responses. The results we found are an important characterization of cellular response to elevated wall shear stress with implications for future models DSS and other LVOT pathologies.

Acknowledgements

Financial support for this research was provided by a gift from Lew and Laura Moorman, NIH R01 HL140305 (to KJGA and SGK), and NSF Graduate Research Fellowship Program (for KNB).

References

1. Darcin OT, Yagdi T, Atay Y, Engin C, Levent E, Buket S, et al. Discrete Subaortic Stenosis. Tex Heart Inst J. 2003;30(4):286–92.
2. Allen HD. Moss and Adams' Heart Disease in Infants, Children, and Adolescents. 9th ed. Vol. I&II. Wolters Kluwer; 2016.
3. Donald JS, Naimo PS, d'Udekem Y, Richardson M, Bullock A, Weintraub RG, et al. Outcomes of Subaortic Obstruction Resection in Children. Heart, Lung and Circulation. 2017 Feb 1;26(2):179–86.
4. Shar JA, Brown KN, Keswani SG, Grande-Allen J, Sucosky P. Impact of Aortoseptal Angle Abnormalities and Discrete Subaortic Stenosis on Left-Ventricular Outflow Tract Hemodynamics: Preliminary Computational Assessment. Front Bioeng Biotechnol. 2020;8:114.

5. Yap SC, Roos-Hesselink JW, Bogers AJJC, Meijboom FJ. Steepened aortoseptal angle may be a risk factor for discrete subaortic stenosis in adults. International Journal of Cardiology. 2008 May;126(1):138–9.

6. Cape EG, VanAuker MD, Sigfússon G, Tacy TA, del Nido PJ. Potential Role of Mechanical Stress in the Etiology of Pediatric Heart Disease: Septal Shear Stress in Subaortic Stenosis. Journal of the American College of Cardiology. 1997 Jul;30(1):247–54.

7. Silbiger J. The Role of Shear Stress in the Pathogenesis of Discrete Subaortic Stenosis: Implications for Surgical Treatment. J Heart Valve Dis. 2011;20(2):123–8.

8. Foker JE. Outcomes and Questions About Discrete Subaortic Stenosis. Circulation. 2013 Apr 9;127(14):1447–50.

9. Butany J, Vaideeswar P, David TE. Discrete subaortic membranes in adults—a clinicopathological analysis. Cardiovascular Pathology. 2009 Jul;18(4):236–42.

10. Heo KS, Lee H, Nigro P, Thomas T, Le NT, Chang E, et al. PKCζ mediates disturbed flow-induced endothelial apoptosis via p53 SUMOylation. J Cell Biol. 2011 May 30;193(5):867–84.

11. Sucosky P, Padala M, Elhammali A, Balachandran K, Jo H, Yoganathan AP. Design of an Ex Vivo Culture System to Investigate the Effects of Shear Stress on Cardiovascular Tissue. Journal of Biomechanical Engineering. 2008;130(3):035001.

12. Li HM, Bi YR, Li Y, Fu R, Lv WC, Jiang N, et al. A potent CBP/p300-Snail interaction inhibitor suppresses tumor growth and metastasis in wild-type p53-expressing cancer. Sci Adv. 2020 Apr 22;6(17):eaaw8500.

13. Goncharov NV, Popova PI, Avdonin PP, Kudryavtsev IV, Serebryakova MK, Korf EA, et al. Markers of Endothelial Cells in Normal and Pathological Conditions. Biochem Moscow Suppl Ser A. 2020 Jul 1;14(3):167–83.

14. Kovacic JC, Dimmeler S, Harvey RP, Finkel T, Aikawa E, Krenning G, et al. Endothelial to Mesenchymal Transition in Cardiovascular Disease: JACC State-of-the-Art Review. J Am Coll Cardiol. 2019 Jan 22;73(2):190–209.
15. Dejana E, Hirschi KK, Simons M. The molecular basis of endothelial cell plasticity. Nat Commun. 2017 Feb 9;8(1):14361.
16. Gong H, Lyu X, Wang Q, Hu M, Zhang X. Endothelial to mesenchymal transition in the cardiovascular system. Life Sciences. 2017 Sep 1;184:95–102.
17. Alvandi Z, Bischoff J. Endothelial-Mesenchymal Transition in Cardiovascular Disease. Arterioscler Thromb Vasc Biol. 2021 Sep;41(9):2357–69.
18. Islam S, Boström KI, Di Carlo D, Simmons CA, Tintut Y, Yao Y, et al. The Mechanobiology of Endothelial-to-Mesenchymal Transition in Cardiovascular Disease. Front Physiol. 2021;12:734215.
19. Peng Q, Shan D, Cui K, Li K, Zhu B, Wu H, et al. The Role of Endothelial-to-Mesenchymal Transition in Cardiovascular Disease. Cells. 2022 Jun 3;11(11):1834.
20. Oh NA, Hong X, Doulamis IP, Meibalan E, Peiseler T, Melero-Martin J, et al. Abnormal Flow Conditions Promote Endocardial Fibroelastosis Via Endothelial-to-Mesenchymal Transition, Which Is Responsive to Losartan Treatment. JACC Basic Transl Sci. 2021 Dec;6(12):984–99.
21. Dahal S, Huang P, Murray BT, Mahler GJ. Endothelial to mesenchymal transformation is induced by altered extracellular matrix in aortic valve endothelial cells. J Biomed Mater Res. 2017 Oct;105(10):2729–41.
22. Feulner L, van Vliet PP, Puceat M, Andelfinger G. Endocardial Regulation of Cardiac Development. J Cardiovasc Dev Dis. 2022 Apr 19;9(5):122.

23. Mahler GJ, Frendl CM, Cao Q, Butcher JT. Effects of shear stress pattern and magnitude on mesenchymal transformation and invasion of aortic valve endothelial cells: Shear Stress Induced EndMT. Biotechnol Bioeng. 2014 Nov;111(11):2326–37.
24. Mahmoud MM, Serbanovic-Canic J, Feng S, Souilhol C, Xing R, Hsiao S, et al. Shear stress induces endothelial-to-mesenchymal transition via the transcription factor Snail. Sci Rep. 2017 13;7(1):3375.
25. Zhang H, Lui KO, Zhou B. Endocardial Cell Plasticity in Cardiac Development, Diseases and Regeneration. Circulation Research. 2018 Mar 2;122(5):774–89.
26. Baulida J, Díaz VM, Herreros AG de. Snail1: A Transcriptional Factor Controlled at Multiple Levels. J Clin Med. 2019 May 28;8(6):E757.
27. McCormick ME, Manduchi E, Witschey WRT, Gorman RC, Gorman JH, Jiang YZ, et al. Spatial phenotyping of the endocardial endothelium as a function of intracardiac hemodynamic shear stress. J Biomech. 2017 Jan 4;50:11–9.
28. Aneesh Kumar A, Ajith Kumar GS, Satheesh G, Surendran A, Chandran M, Kartha CC, et al. Proteomics Analysis Reveals Diverse Molecular Characteristics between Endocardial and Aortic-Valvular Endothelium. Genes (Basel). 2021 Jun 30;12(7):1005.
29. Jaleel A, Aneesh Kumar A, Ajith Kumar GS, Surendran A, Kartha CC. Label-free quantitative proteomics analysis reveals distinct molecular characteristics in endocardial endothelium. Mol Cell Biochem. 2019 Jan;451(1–2):1–10.
30. McCormick ME, Manduchi E, Witschey WRT, Gorman RC, Gorman JH, Jiang Y, et al. Integrated Regional Cardiac Hemodynamic Imaging and RNA Sequencing Reveal Corresponding Heterogeneity of Ventricular Wall Shear Stress and Endocardial Transcriptome. J Am Heart Assoc [Internet]. 2016 Apr 18 [cited 2018 Jul 4];5(4). Available from: https://www.ncbi.nlm.nih.gov/pmc/articles/PMC4859290/

31. Moonen JRAJ, Lee ES, Schmidt M, Maleszewska M, Koerts JA, Brouwer LA, et al. Endothelial-to-mesenchymal transition contributes to fibro-proliferative vascular disease and is modulated by fluid shear stress. Cardiovasc Res. 2015 Dec 1;108(3):377–86.
32. Ajami NE, Gupta S, Maurya MR, Nguyen P, Li JYS, Shyy JYJ, et al. Systems biology analysis of longitudinal functional response of endothelial cells to shear stress. Proc Natl Acad Sci U S A. 2017 Oct 10;114(41):10990–5.
33. Serbanovic-Canic J, Souilhol C, Evans PC. Shear stress makes its mark on the endothelial genome. Cardiovasc Res. 2019 Aug 1;115(10):1449–51.
34. Silvani G, Romanov V, Cox CD, Martinac B. Biomechanical Characterization of Endothelial Cells Exposed to Shear Stress Using Acoustic Force Spectroscopy. Frontiers in Bioengineering and Biotechnology [Internet]. 2021 [cited 2022 Oct 29];9. Available from: https://www.frontiersin.org/articles/10.3389/fbioe.2021.612151
35. Maurya MR, Gupta S, Li JYS, Ajami NE, Chen ZB, Shyy JYJ, et al. Longitudinal shear stress response in human endothelial cells to atheroprone and atheroprotective conditions. Proceedings of the National Academy of Sciences. 2021 Jan 26;118(4):e2023236118.
36. Li Af, Tan L, Zhang S, Tao J, Wang Z, Wei D. Low shear stress-induced endothelial mesenchymal transformation via the down-regulation of TET2. Biochemical & Biophysical Research Communications. 2021 Mar 19;545:20–6.

Table 1. Cone-and-plate Device Settings

Rotational Speed Setting (RPM)	**Shear Stress Applied** (dynes/cm^2)
280	15
370	20
660	35

Table 2. Antibody information and concentrations used for flow cytometry.

Antibody Information	**Amount of Antibody Added to 100 μL Sample**
Extracellular Proteins	
CD31 Monoclonal Antibody (LCI-4) [APC] – Thermo Fisher, #MA5-16769	10 μL
Mouse IgG1 kappa Isotype Control [APC] – Thermo Fisher, #17-4714-42	5 μL
VCAM-1 Monoclonal Antibody (1.G11B1) [FITC] – Thermo Fisher, #MA5-16430	4 μL
Igg1, K Mouse, Clone: P3.6.2.8.1, Isotype Control [FITC] – Thermo Fisher, #11-4714-42	4 μL
CD62E/CD62P Monoclonal Antibody (1.2B6) [PE] – Thermo Fisher, #MA5-28649	4 μL
Mouse IgG1 Isotype Control [PE] – Thermo Fisher, #MA518097	4 μL
Intracellular Proteins	
Snail Antibody [AlexaFluor® 750] – Novus Biologicals, # NBP2-27293AF750	4 μL
Rabbit IgG Isotype Control [AlexaFluor 750] – Novus Biologicals, # NBP2-24891AF750	4 μL
Vimentin Antibody (RV203) [PerCP] – Novus Biologicals, # NBP1-97671PCP	4 μL
Mouse IgG1 Isotype control [PerCP] – Novus Biologicals, # IC002C	4 μL
α-Smooth Muscle Actin Antibody [AlexaFluor 405] – Novus Biologicals, # NBP2-34522AF405	4 μL
Mouse IgG2a Isotype Control (M2AK) [AlexaFluor 405] – Novus Biologicals, # NBP1-96981AF405	4 μL

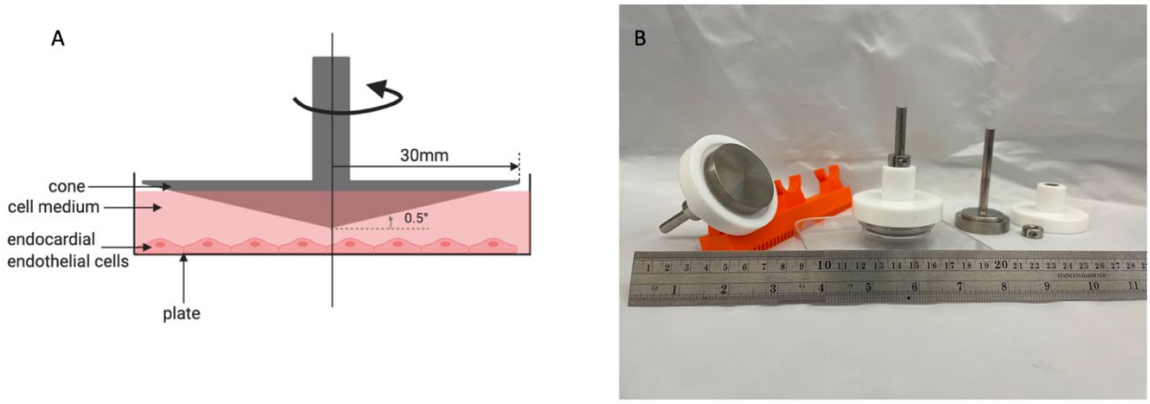

Figure 1. Cone-and-plate Device. (A) Illustration of the cone-and-plate device. Endocardial endothelial cells are grown in a monolayer in a 60 mm petri dish, and the cone is loaded onto the petri dish containing the cells and cell culture medium and rotated using a controllable magnetic stir plate. (B) Photo of the cone and Teflon cover setup used in the shear stress studies. On the left of the photo, the cone is supported by a 3D printed holding device, which is used to position multiple cones towards a UV light for sterilization prior to use. In the center of the photo, the cone is loaded onto a petri dish. On the right of the photo, the cone, Teflon cover, and shaft collar are disassembled to show the individual parts used in the setup.

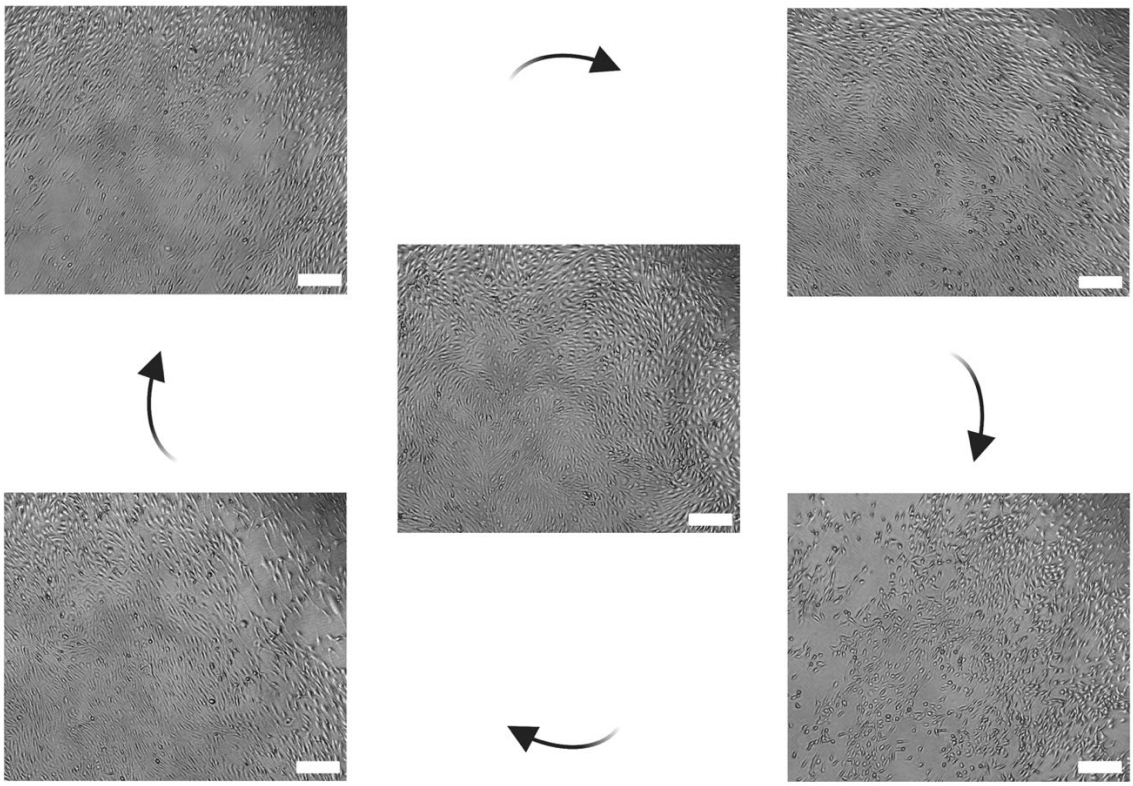

Figure 2. Brightfield images of EECs after exposure to high shear stress. Images of each sample were taken at 5 different locations around the petri dish. A representative set of images of a single sample is shown. The arrows show the direction of shear stress applied to this sample. Scale bar shown is 200 μm.

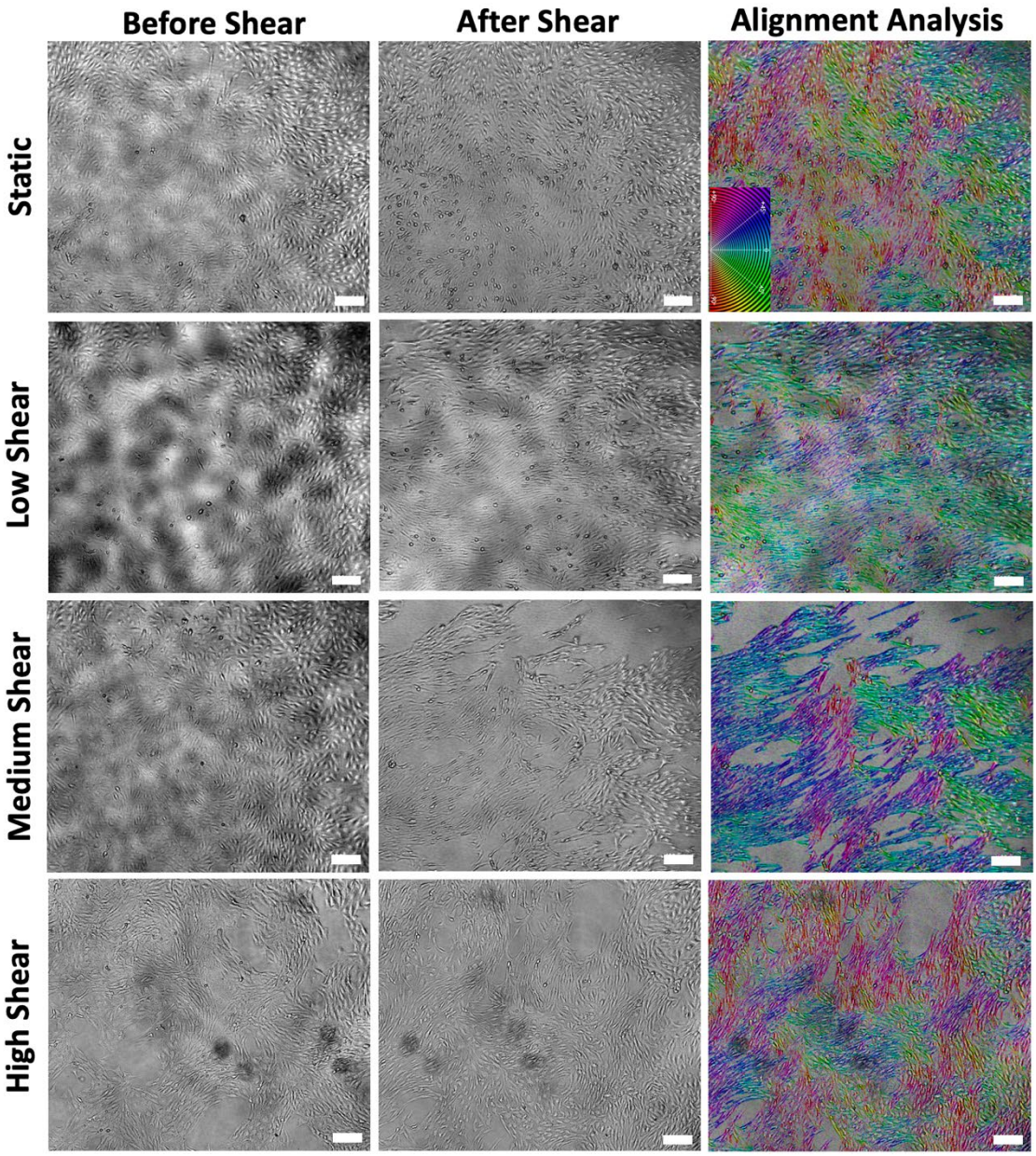

Figure 3. Brightfield images of EECs before and after exposure to shear stress. The rows compare EECs exposed to static conditions and low, medium, and high shear stresses. The last column of the panel shows the color mapping of EECs to measure their alignment after exposure to shear stress. The color map code (see inset of static condition) is provided to show how the alignment of the cells corresponds to color and thereby orientation. Scale bar shown is 200 μm. These were individual samples analyzed at the same location on the petri dish. Data shown in figure is representative of all data collected.

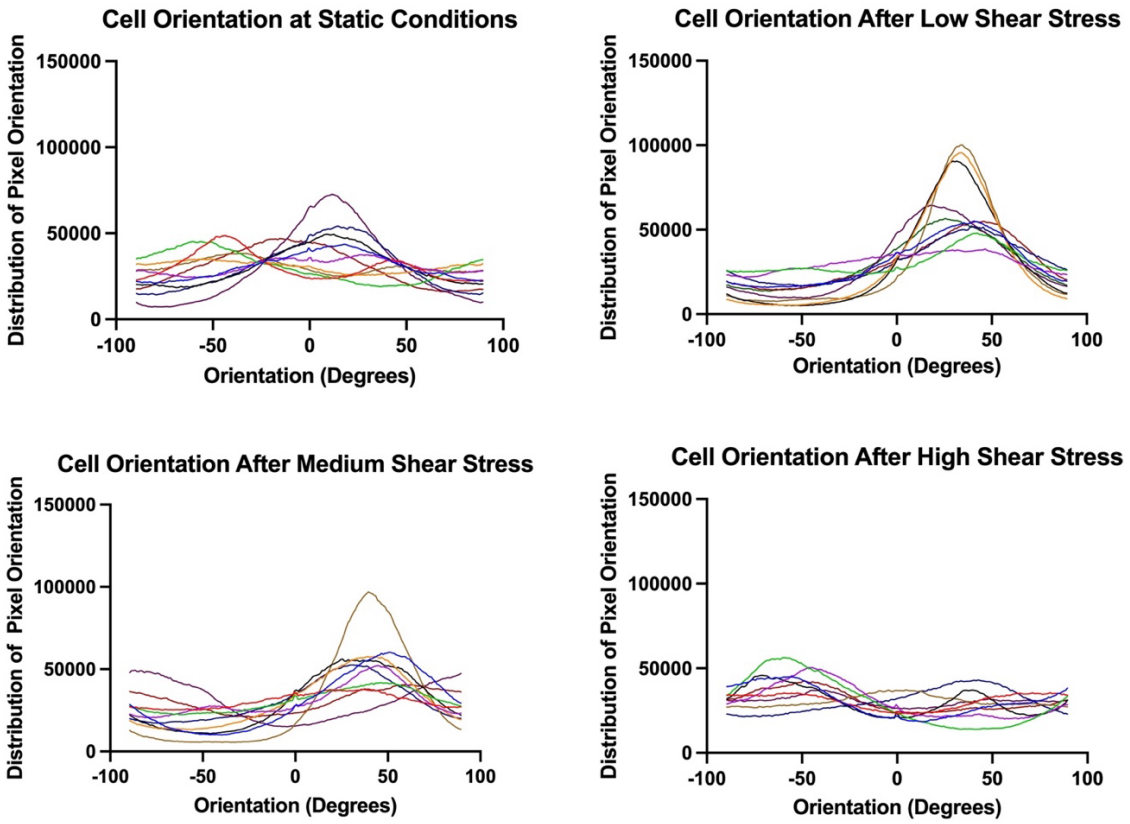

Figure 4. The cell orientation of 10 samples of imaged EECs was analyzed for each shear condition to compare their distribution of orientation across shear rates. Each line represents an individual sample analyzed at the same location on the petri dish. Data shown in figure is representative of all data collected.

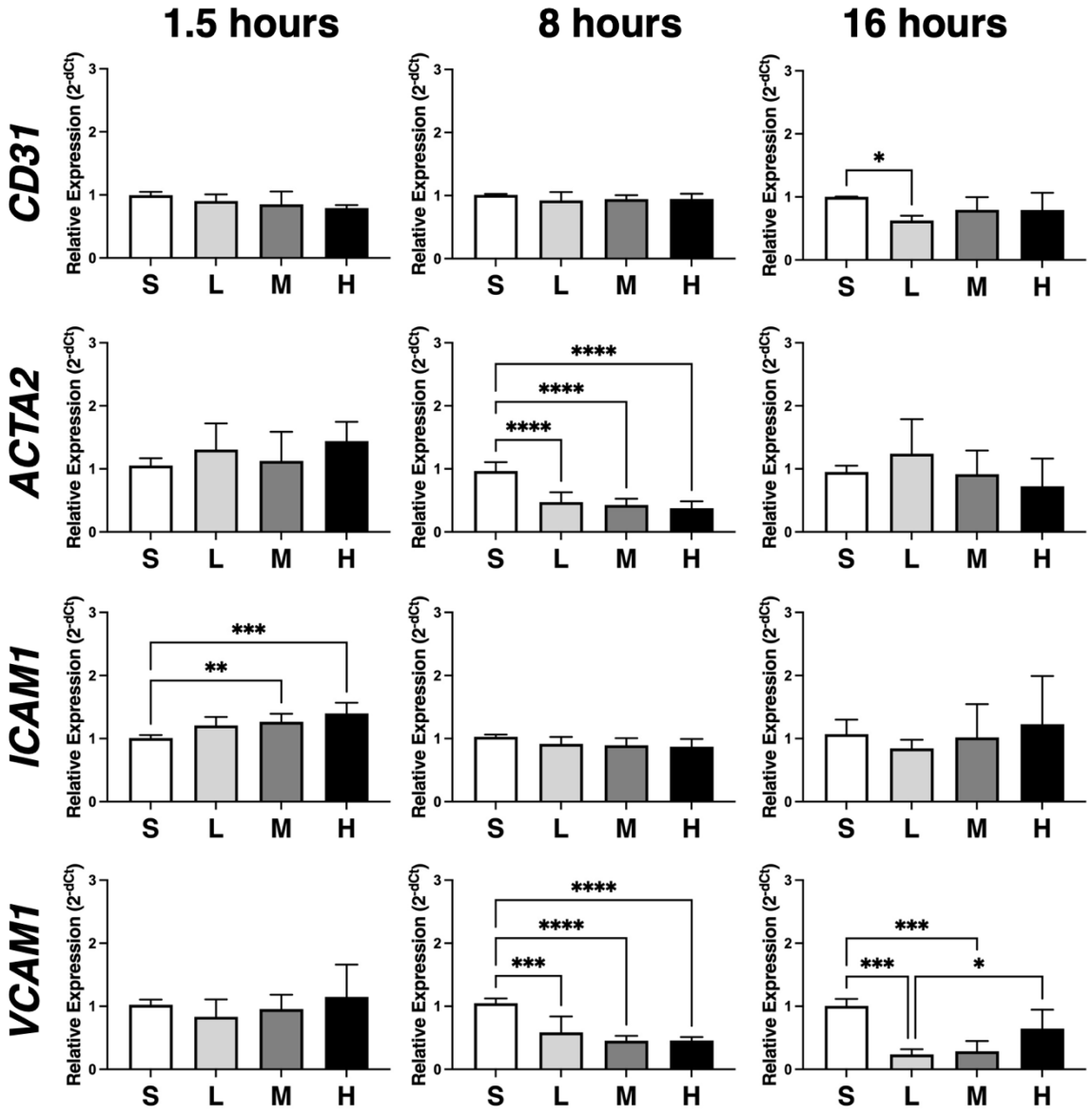

Figure 5. PCR results that compare the gene expression of EECS under static (S), low shear (L), medium shear (M), and high shear (H) conditions. The rows show expression of *CD31*, *ACTA2*, *ICAM1*, and *VCAM1*. The columns show the expression of the cells at 1.5-hour, 8-hour, and 16-hour time points. The statistical analysis performed on the samples was a one-way ANOVA. Sample size was n=3. Data is expressed as mean $\pm$ standard deviation (SD). * indicates the p value was between 0.01-0.05, ** indicates the p value was between 0.001-0.01, *** indicates the p value was between 0.0001-0.001, and **** indicates the p value was less than 0.0001.

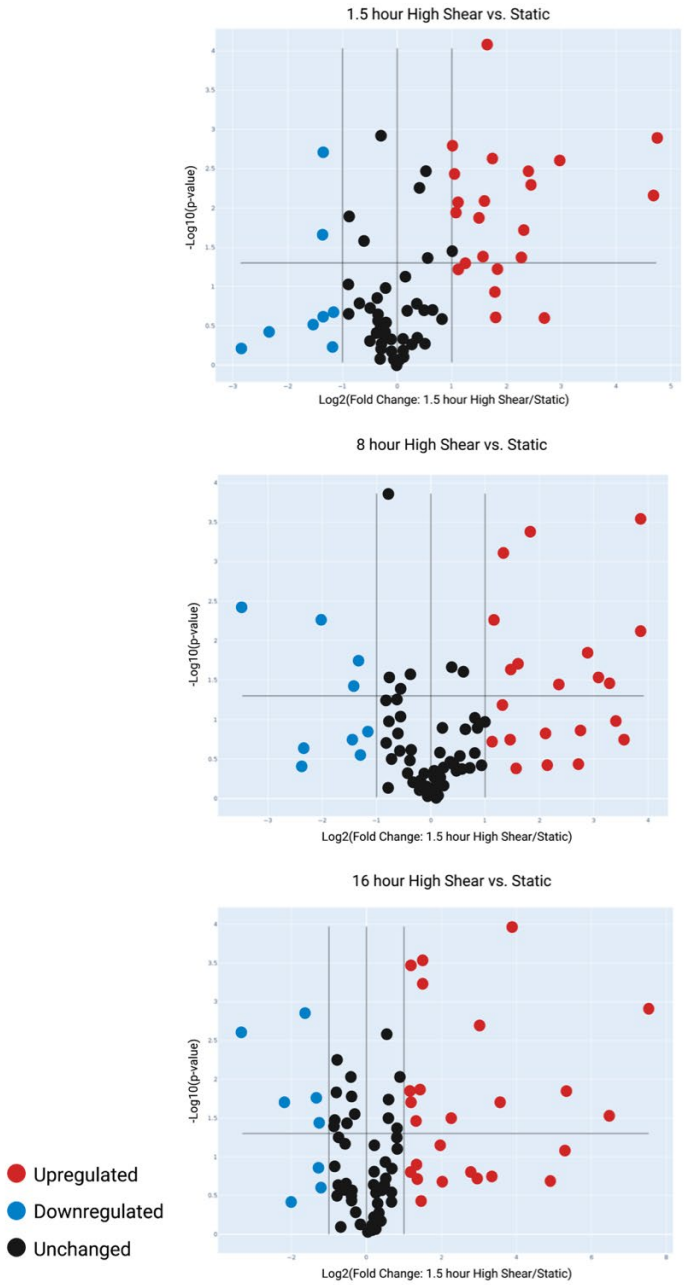

Figure 6. Volcano plots comparing the gene expression of static EECs to EECs exposed to high shear stress at 1.5, 8, and 16 hours, respectively. Genes that are significantly upregulated are shown as red dots, genes that are significantly downregulated are shown as blue dots, and genes that remain unchanged are shown as black dots.

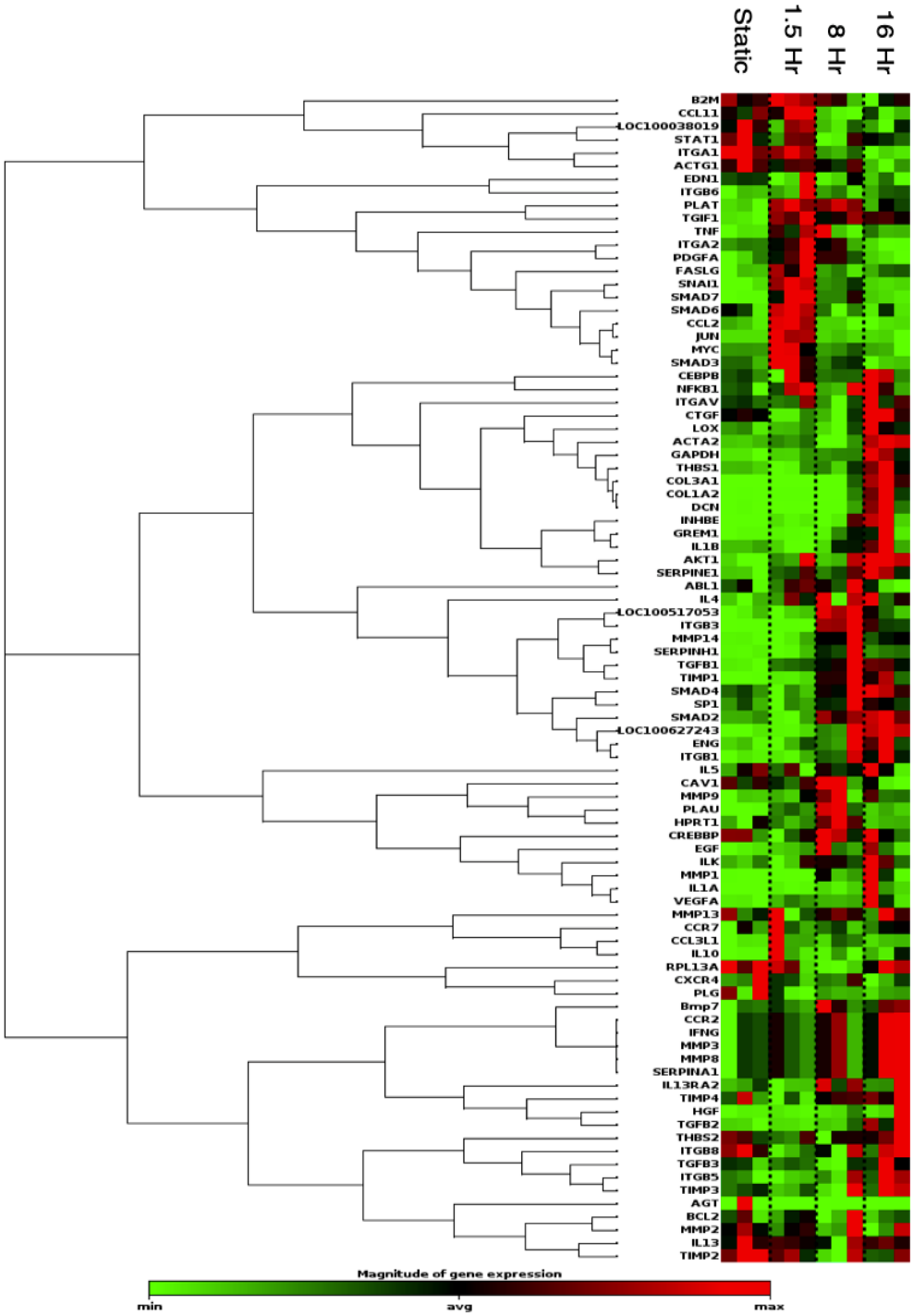

Figure 7. Clustergram from the fibrosis profiler array comparing the gene expression of static EECs to EECs exposed to high shear stress at 1.5, 8, and 16 hours, respectively. The samples are grouped by shear condition and time point. Green = minimum magnitude of gene expression; Red = maximum magnitude of gene expression.

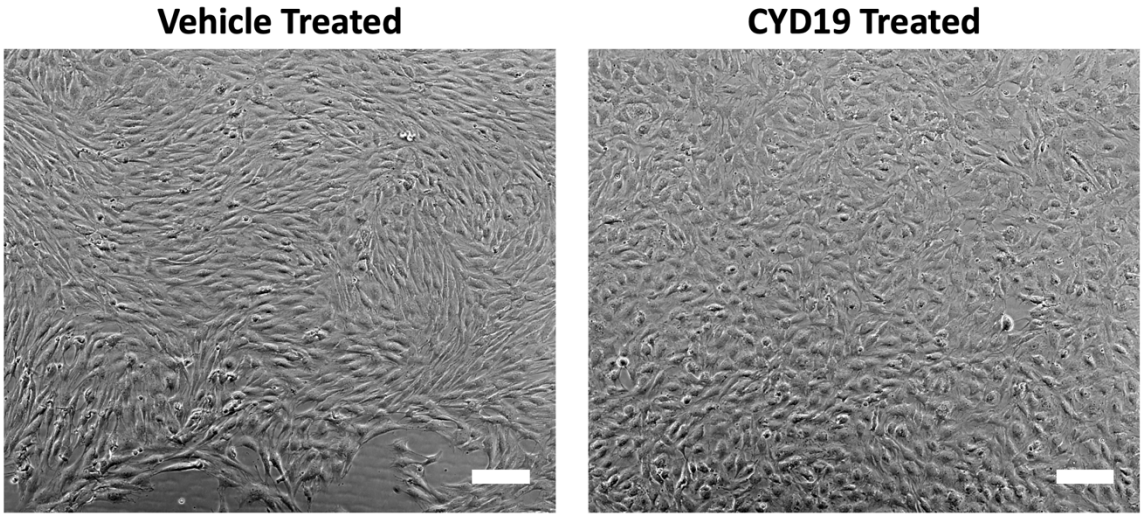

Figure 8. Comparison of vehicle-treated EECs (left) and CYD19-treated EECs (right). Scale bar = 100 µm.

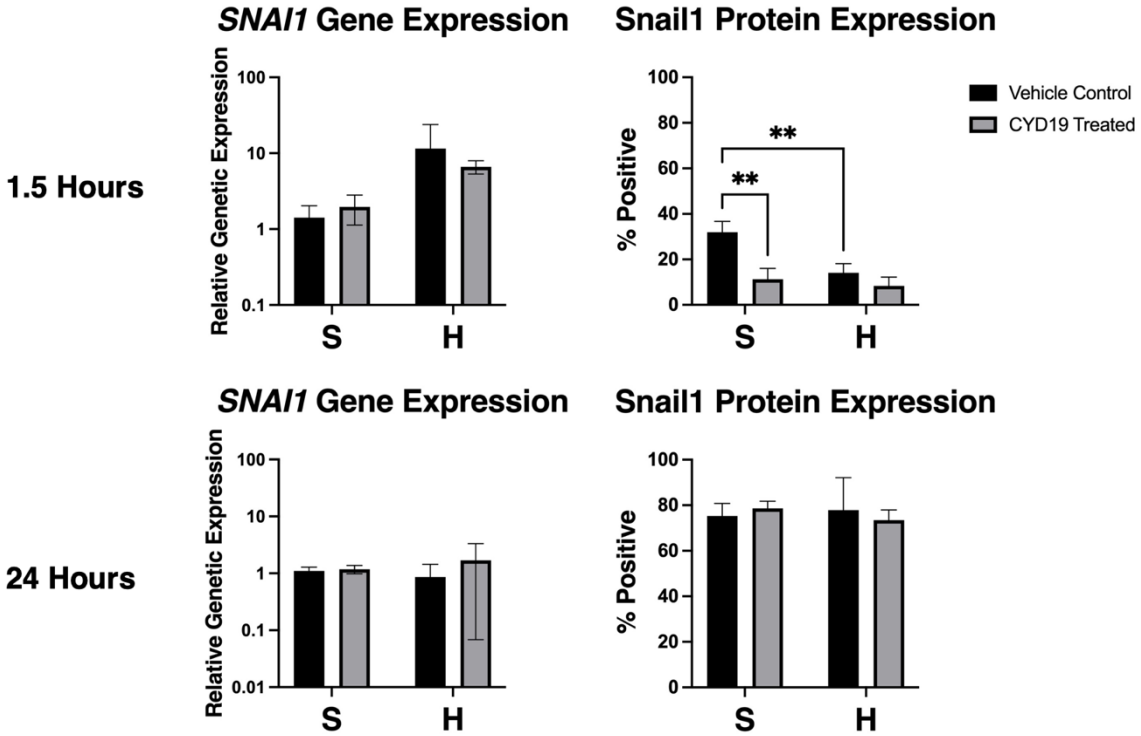

Figure 9. Gene and protein expression of Snail from EECs cultured under either static conditions or high shear stress, and treated with either vehicle control or the small molecule inhibitor CYD19 at 1.5 hours and 24 hours. Data is expressed as mean $\pm$ standard deviation. *p between 0.01-0.05, **p between 0.001-0.01, ***p between 0.0001-0.001, and ****p <0.0001.

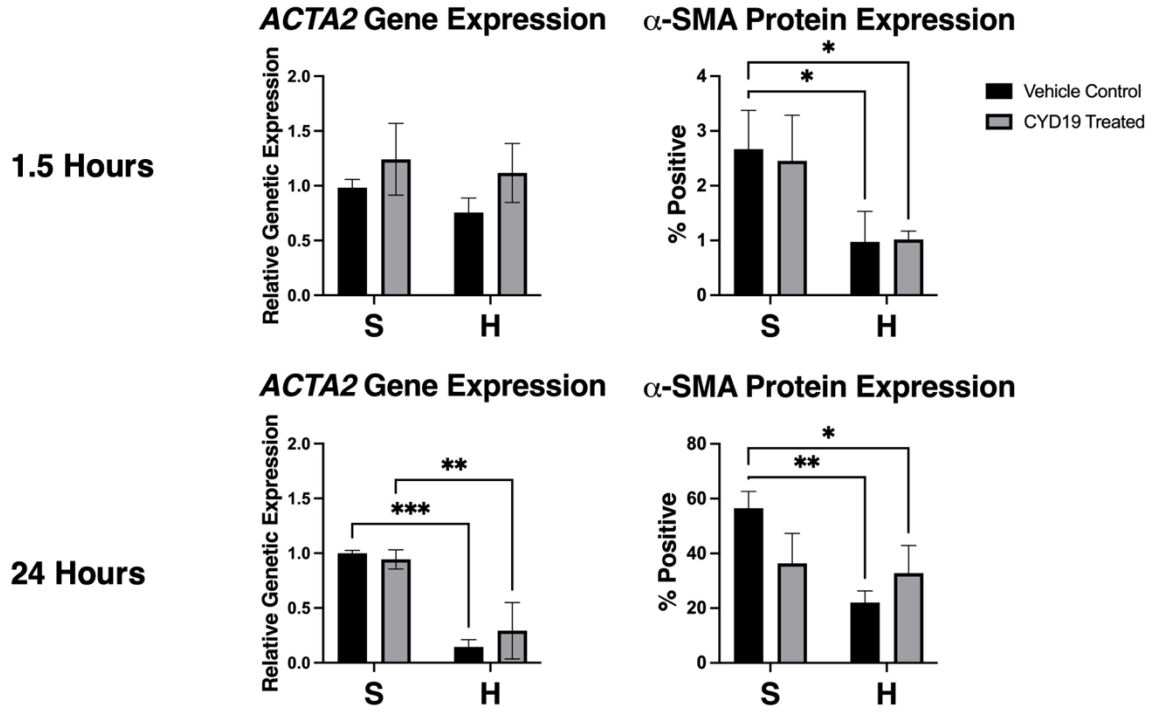

Figure 10. Gene and protein expression of α-smooth muscle actin from EECs cultured under either static conditions or high shear stress, and treated with either vehicle control or the small molecule inhibitor CYD19 at 1.5 hours and 24 hours. Data is expressed as mean $\pm$ standard deviation (SD). *p between 0.01-0.05, **p between 0.001-0.01, ***p between 0.0001-0.001, and ****p < 0.0001.

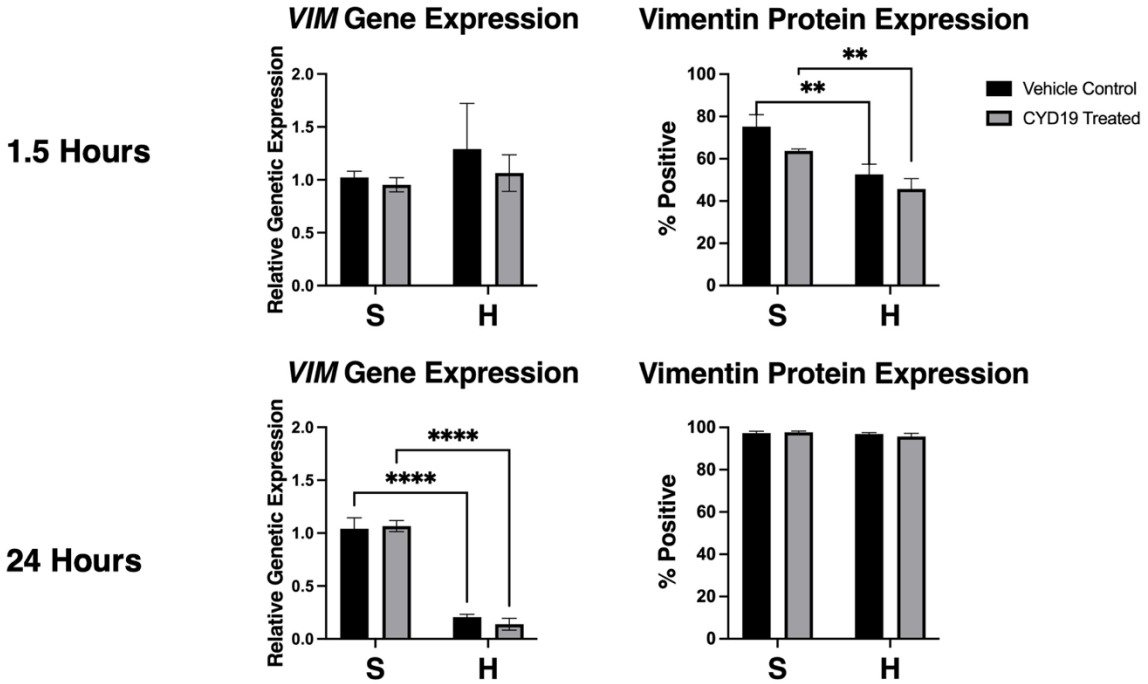

Figure 11. Gene and protein expression of Vimentin from EECs cultured under either static conditions or high shear stress, and treated with either vehicle control or the small molecule inhibitor CYD19 at 1.5 hours and 24 hours. Data is expressed as mean $\pm$ standard deviation (SD). *p between 0.01-0.05, **p between 0.001-0.01, ***p between 0.0001-0.001, and ****p < 0.0001.

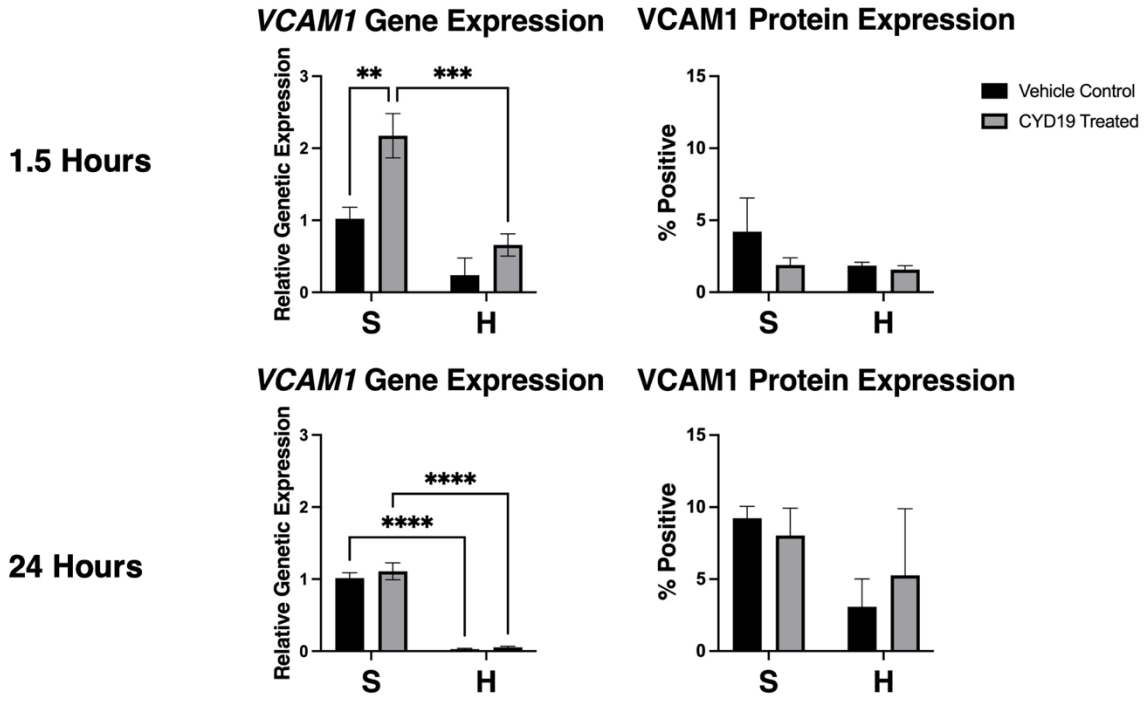

Figure 12. Gene and protein expression of VCAM1 from EECs cultured under either static conditions or high shear stress, and treated with either vehicle control or the small molecule inhibitor CYD19 at 1.5 and 24 hours. Data is expressed as mean ± standard deviation. *p between 0.01-0.05, **p between 0.001-0.01, ***p between 0.0001-0.001, and ****p < 0.0001.

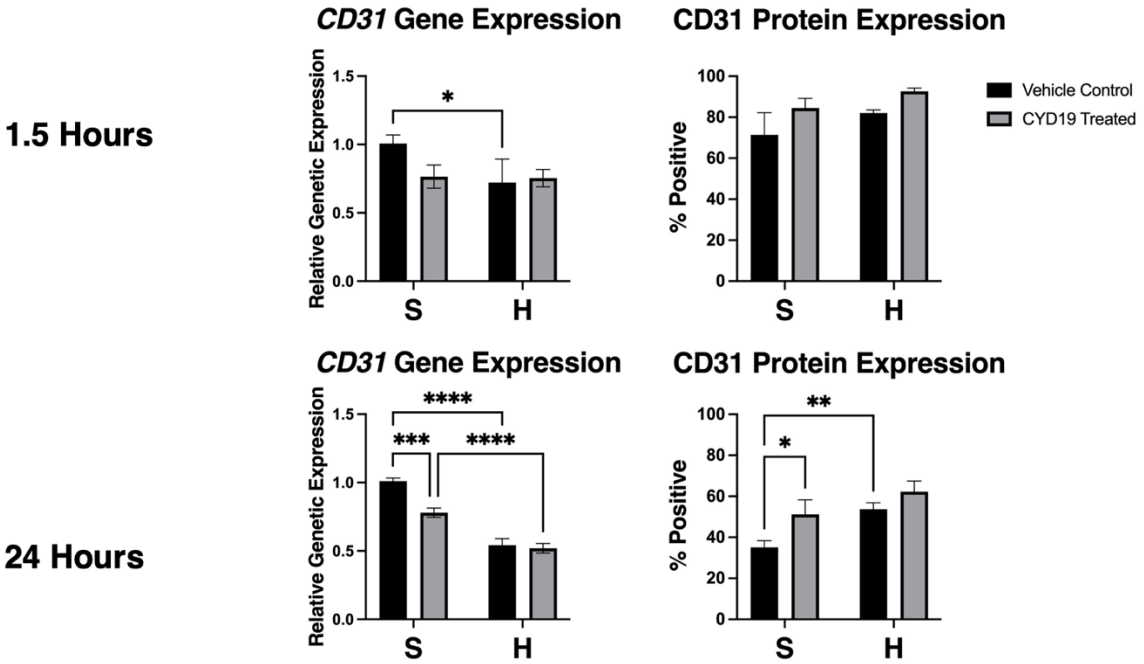

Figure 13. Gene and protein expression of CD31 from EECs cultured under either static conditions or high shear stress, and treated with either vehicle control or the small molecule inhibitor CYD19 at 1.5 and 24 hours. Data is expressed as mean ± standard deviation. * p between 0.01-0.05, **p between 0.001-0.01, ***p between 0.0001-0.001, and ****p < 0.0001.